Supplementary Information

IRAK2 deficiency causes immune dysregulation through defective Myddosome assembly and enhanced interferon responses

Yudie Fei[1, 2, #], Lin Liu[3, 4, #], Shuangyue Ma[1, #], Ying Jin[5, #], Shihao Wang[1, 6, #], Liang Zhang[7, 8, 9, 10, #], Jun Yang[11, #], Yi Liu[12, #], Meiping Lu[13, #], Jing Xue[14, #], Jingyi Li[15, #], Xiang Chen[1, #], Jun Wang[1, 16, #], Yuhao Yao[4, #], Chenlu Liu[4, #], Jiahui Zhang[2, #], Xu Han[1, 16, 17, #], Jinjian Fu[4, #], Zhijuan Kang[7, 8, 9, 10, #], Yusha Wang[1, 16], Xiangwei Sun[1], Changming Zhang[2], Tingyan He[11], Zhihui Liu[12], Li Guo[13], Chengshun Chen[15], Hongmei Zhao[18], Xingjian Gao[2], Hua Zhong[14], Lihong Wen[14], Xiaomin Yu[1, 14, *, +], Zhihong Liu[5, 1, *, +], Qing Zhou[1, 4, 16, 19, *, +]

1 Liangzhu Laboratory, Zhejiang University, Hangzhou, China

2 National Clinical Research Center for Kidney Diseases, Jinling Hospital, Affiliated Hospital of Medical School, Nanjing University, Nanjing, China

3 Urology & Nephrology Center, Department of Nephrology, Zhejiang Provincial People's Hospital (Affiliated People's Hospital, Hangzhou Medical College), Hangzhou, China

4 Life Sciences Institute, Zhejiang University, Hangzhou, China

5 National Clinical Research Center of Kidney Diseases, Jinling Clinical Medical College, Nanjing Medical University, Nanjing, China

6 Cell and Molecular Biology Laboratory, Affiliated Zhoushan Hospital of Wenzhou Medical University, Zhoushan, China

7 The Affiliated Children's Hospital of Xiangya School of Medicine, Central South University (Hunan Children's Hospital), Changsha, Hunan, China

8 Department of Nephrology, Rheumatology and Immunology, Hunan Children's Hospital, Changsha, Hunan, China

9 The School of Pediatrics, Hengyang Medical School, University of South China, Hengyang 421001, Hunan, China

10 Hunan Provincial Key Laboratory of Pediatric Orthopedics, Changsha, Hunan, China

11 Department of Rheumatology and Immunology, Shenzhen Children's Hospital, Shenzhen, China

12 Department of Rheumatology and Immunology, West China Hospital, Sichuan University, Chengdu, China

13 Department of Rheumatology Immunology and Allergy, Children's Hospital, Zhejiang University School of Medicine, Hangzhou, China

14 Department of Rheumatology, The Second Affiliated Hospital, Zhejiang University School of Medicine, Hangzhou, Zhejiang, China

15 Department of Rheumatology and Immunology, The First Hospital Affiliated to The Army Medical University (Third Military Medical University), Chongqing, China

16 Department of Rheumatology, Sir Run Run Shaw Hospital, Zhejiang University School of Medicine, Hangzhou, China

17 Hangzhou Institute of Medicine, Chinese Academy of Sciences, Hangzhou, China

18 Department of Digestive Nutrition, Hunan Children's Hospital, Changsha, China

19 State Key Laboratory of Common Mechanism Research for Major Diseases, Institute of Basic Medical Sciences & School of Basic Medicine, Chinese Academy of Medical Sciences & Peking Union Medical College, Beijing, China

#These authors contributed equally: Yudie Fei, Lin Liu, Shuangyue Ma, Ying Jin, Shihao Wang, Liang Zhang, Jun Yang, Yi Liu, Meiping Lu, Jing Xue, Jingyi Li, Xiang Chen, Jun Wang, Yuhao Yao, Chenlu Liu, Jiahui Zhang, Xu Han, Jinjian Fu, Zhijuan Kang.

*These authors jointly supervised this work: Qing Zhou, Zhihong Liu, Xiaomin Yu.

[+]Corresponding authors: zhouqingnwu@gmail.com; liuzhihong@zju.edu.cn; yuxiaomin@zju.edu.cn.

This Supplementary Information file contains: Supplementary Patient Information, Supplementary Figures 1-11, Supplementary Tables 1-5 and Supplementary References.

Supplementary Patient Information

The DIRAK2 cohort consists of twelve patients from eleven unrelated families (Fig. 1a and Supplementary Table 1).

Patient 1 (P1) was a 15-year-old girl born to non-consanguineous parents. She presented in infancy with cough, sputum production, shortness of breath, inspiratory stridor, weak crying, and feeding difficulties. She was diagnosed with pneumonia and treated with antibiotics. Marked motor delay was noted, including absent head control at 3 months of age, attributed to generalized weakness and hypotonia, necessitating rehabilitation therapy. She also had delayed mental and intellectual development. Since then, she has suffered from recurrent suppurative pneumonia (Fig. 1b), otitis media, and sinusitis, with culture-confirmed infections due to Gram-positive or Gram-negative bacteria, viruses, and fungi (Supplementary Table 2). Computed tomographic (CT) scan showed bronchiectasis with infection in the right lower lobe, accompanied by mucus plugging within the bronchial lumen and adjacent pleural traction with thickening. Atelectasis of the right middle lobe. Mild residual fibrotic lesions in both lungs, consistent with prior inflammatory changes (Fig. 1b). All known primary immunodeficiencies (PIDs) were excluded after genetic testing with whole exome sequencing (WES). Based on the history of recurrent polymicrobial infections, she was diagnosed with PID. Management included hospitalization for infection control with fiberoptic bronchoscopy and targeted antimicrobial therapy based on culture results. Prophylactic intravenous immunoglobulin (IVIG) was administered to address the underlying immunodeficiency. Notably, the frequency of infections decreased after the age of 10 years, suggesting partial immune maturation.

P2 experienced recurrent pulmonary infections from the age of 49 years. She was admitted at the age of 64 years due to recurrent fever and cough lasting for more than

2 months (Fig. 1c). On admission, laboratory evaluation revealed hypogammaglobulinemia (Supplementary Table 3) and immune cytopenia. Peripheral blood CMV DNA was positive by quantitative real-time PCR, with a viral load of 1.18×10^5 copies/mL, consistent with CMV viremia (systemic infection). CMV serology (positive IgM with low IgG) supported a primary CMV infection. She died of severe pneumonia at the age of 65 years. Microbiologic evaluation revealed polymicrobial infections involving Gram-negative bacteria, as well as viral and fungal pathogens (Supplementary Table 2). In the 6 months preceding death, she also developed systemic arthralgia. Treatment included anti-infective treatment with antibiotics, anti-inflammatory treatment with methylprednisolone, and IVIG administration.

P3 was a 49-year-old female who first presented with swelling of both lower limbs, butterfly facial erythema, hair loss, arthralgia, proteinuria, and thrombocytopenia at the age of 22 years. She was prescribed with prednisone and cyclophosphamide (CTX) and received complete remission. At the age of 34 years, she underwent disease relapse, characterized by proteinuria, hematuria, pancytopenia, positive autoantibodies, and decreased C3 level. Based on these findings, she was diagnosed with systemic lupus erythematosus (SLE) according to the European Alliance of Associations for Rheumatology/American College of Rheumatology classification criteria.[1] Kidney biopsy revealed the class IV+V lupus nephritis (Fig. 1d-f and Supplementary Fig. 1a). Prednisone combined with CTX pulse treatment (9.3 g in total) resulted in partial remission. Then prednisone, azathioprine (AZA) or mycophenolate mofetil (MMF), and hydroxychloroquine (HCQ) were prescribed. Complete remission was achieved and maintained until the last visit. Despite her autoimmune manifestations, she was found to have hypogammaglobulinemia (Supplementary Table 3). At the age of 48 years, she experienced severe COVID-19 pneumonia. During the follow-up period, she reported recurrent conjunctivitis and pruritic skin lesions associated with viral warts.

P4, P3's 22-year-old daughter, had mild symptoms, including occasional skin rashes around the waist and hair loss. Antinuclear antibody (ANA) testing was positive (Supplementary Table 3), and the type I interferon (IFN) signature was elevated, both of which increased over time and showed a strong correlation (Supplementary Fig. 1c). Additional autoantibodies, including anti-β2 glycoprotein I (A-β2-GP1) and anti-cardiolipin (ACL) antibodies, were also positive (Supplementary Table 3). She has not received any treatment to date. Both P3 and P4 exhibited an expansion of the $CD8^+$ T cell population (Supplementary Fig. 4a-c), which was notable given that SLE and hair loss were closely associated with elevated IFN signatures and increased $CD8^+$ T cells.[2-4]

P5 was a 20-year-old female. She initially presented with purpuric rashes on both lower limbs, accompanied by swelling of the hands and feet, myalgia, and arthralgia at the age of 13 years. Laboratory tests revealed thrombocytopenia, anemia, proteinuria, occult hematuria, and decreased serum levels of C3 and C4 (Supplementary Table 3). The ANA and anti-dsDNA antibodies were positive (Supplementary Table 3). Kidney biopsy revealed the class V lupus nephritis (Supplementary Fig. 1b). Based on these findings, she was diagnosed with SLE accompanied by lupus nephritis. She was treated with methylprednisolone, HCQ, and tacrolimus, and achieved complete remission. At the age of 16 years, she experienced a disease flare characterized by arthralgia, proteinuria, and occult hematuria, accompanied by an increase in $CD8^+$ T cells, accounting for 39.91% of peripheral blood mononuclear cells (PBMCs). She was prescribed with prednisone, HCQ, tacrolimus, and MMF. Three months later, she underwent infection-induced lupus flare and was treated with belimumab. She remained in complete remission up to her most recent evaluation this year.

P6 was a 12-year-old girl, who initially presented with fatigue, anorexia, butterfly facial erythema, and hair loss at the age of 10 years. The laboratory tests showed leukopenia and anemia (Supplementary Table 3). The ANA test was positive. The CT scan revealed multiple enlarged lymph nodes in the mediastinum, bilateral supraclavicular fossae, axillary regions, abdomen, and retroperitoneum. Ultrasound examination revealed pericardial effusion, splenomegaly, and bilateral suprapatellar joint effusion. She was diagnosed with SLE and treated with glucocorticoid, HCQ, MMF, and telitacicept. At the age of 11 years, she developed herpes zoster followed by pneumonia due to *haemophilus influenzae* subsequently.

P7 was a 61-year-old male, who had experienced recurrent epistaxis associated with thrombocytopenia since the age of 51 years, followed by scattered petechiae and purpura on face, limbs, and trunk, along with oral ulcers and arthralgia. Laboratory tests revealed pancytopenia, hematuria, proteinuria, elevated levels of serum creatinine, decreased levels of C3 and C4, positive ANA, anti-dsDNA antibodies, and antiphospholipid (APL) antibodies (Supplementary Table 3). Inflammatory markers, including C-reactive protein (CRP) and erythrocyte sedimentation rate (ESR), were also elevated (Supplementary Table 3). He was diagnosed with SLE accompanied by lupus nephritis and was treated with prednisone and sirolimus, which effectively controlled the disease activity.

P8 was a 9-year-old boy. He initially presented with recurrent abdominal pain and vomiting, accompanied by hematochezia at the age of 6 years. The patient underwent esophagogastroduodenoscopy (EGD) and colonoscopy, which revealed multiple ulcers throughout the entire gastrointestinal (GI) tract, along with mucosal hyperemia and edema (Fig. 1g). Histopathological examination revealed predominantly inflammatory changes, most pronounced in the terminal ileum. Focal ulcerations with

numerous crypt abscesses were observed (Fig. 1h). Notably, there was no histologic evidence of vasculitis or fibrinoid necrosis. Based on the clinical presentation, endoscopic findings, and histologic features, a diagnosis of inflammatory bowel disease (IBD) was established. He was initially treated with 40 mg methylprednisolone, which was gradually tapered in 6 weeks, and 5 mg/kg infliximab administered at weeks 0, 2, and 6, and then every 8 weeks. The patient's symptoms improved. However, follow-up colonoscopy revealed persistent multiple ulcers throughout the colon and ileocecal region.

P9 was a 22-year-old male who has experienced recurrent episodes of fever and abdominal pain since the age of 14 years, and developed oral and genital ulcers beginning at the age of 17 years, accompanied by skin lesions and proteinuria. A colonoscopy performed at the age of 21 years revealed multiple inflammatory polyps in the ileocecal region and ascending colon (Supplementary Fig. 1d), and histopathologic examination showed chronic mucosal inflammation (Supplementary Fig. 1e). During the disease course, the patient exhibited signs of intestinal obstruction, characterized by abdominal pain, vomiting, and constipation. CRP and ESR were elevated during febrile episodes at the age of 21 years (Supplementary Table 3). He had a medical history of perianal abscess. His clinical manifestations resembled Behçet's disease (BD). The patient was treated with glucocorticoids, combined with CTX or AZA, and vitamin D.

P10 was a 10-year-old girl. She initially presented with left knee pain, accompanied by localized swelling, elevated skin temperature, and inability to ambulate at the age of 4 years. During the disease course, she developed scattered, non-pruritic punctate erythematous rashes on the face, oral ulcers, and rashes on the legs. Magnetic resonance imaging (MRI) showed left knee joint effusion with hemarthrosis accompanied by synovial thickening and enhancement. Abnormal signal intensity was

observed in the left ilium adjacent to the S2-level sacroiliac joint (Fig. 1i). Bilateral hip joints exhibited mild effusions with synovial membrane thickening. Cranial MRI showed evidence of left-sided sinusitis. She was diagnosed with juvenile idiopathic arthritis (JIA) and received sequential treatment with dexamethasone, ibuprofen, and methotrexate (MTX), followed by maintenance monotherapy with MTX (7.5 mg weekly). The patient showed improvement in joint symptoms and complete resolution of skin manifestations.

P11 was a 20-year-old male. He presented with asymptomatic thyroid enlargement. Laboratory tests revealed elevated levels of anti-thyroglobulin (TG) and anti-thyroid peroxidase (TPO) antibodies (Supplementary Table 3), along with an increased thyroid-stimulating hormone (TSH) level. He was diagnosed with Hashimoto's thyroiditis. Additionally, he had cutaneous manifestations consistent with lichen planus. He has not received any treatment to date.

P12 was a 14-year-old girl. The patient presented with sudden-onset syncope accompanied by cyanotic lips and loss of consciousness. Laboratory tests revealed leukocytosis and elevated CRP (Supplementary Table 3). Cranial MRI demonstrated heterogeneous and markedly enhanced signals in the bilateral basal ganglia, with gyriform enhancement in the right frontal lobe and bilateral temporo-occipital lobes. The lateral ventricle on one side appeared slightly enlarged relative to the contralateral side (Supplementary Fig. 1f). She was treated with endotracheal intubation and mechanical ventilatory support, along with intravenous mannitol, dexamethasone (10 mg once daily for 5 days), antimicrobial prophylaxis, and neuroprotective agents including idebenone and mecobalamin.

Supplementary Figures

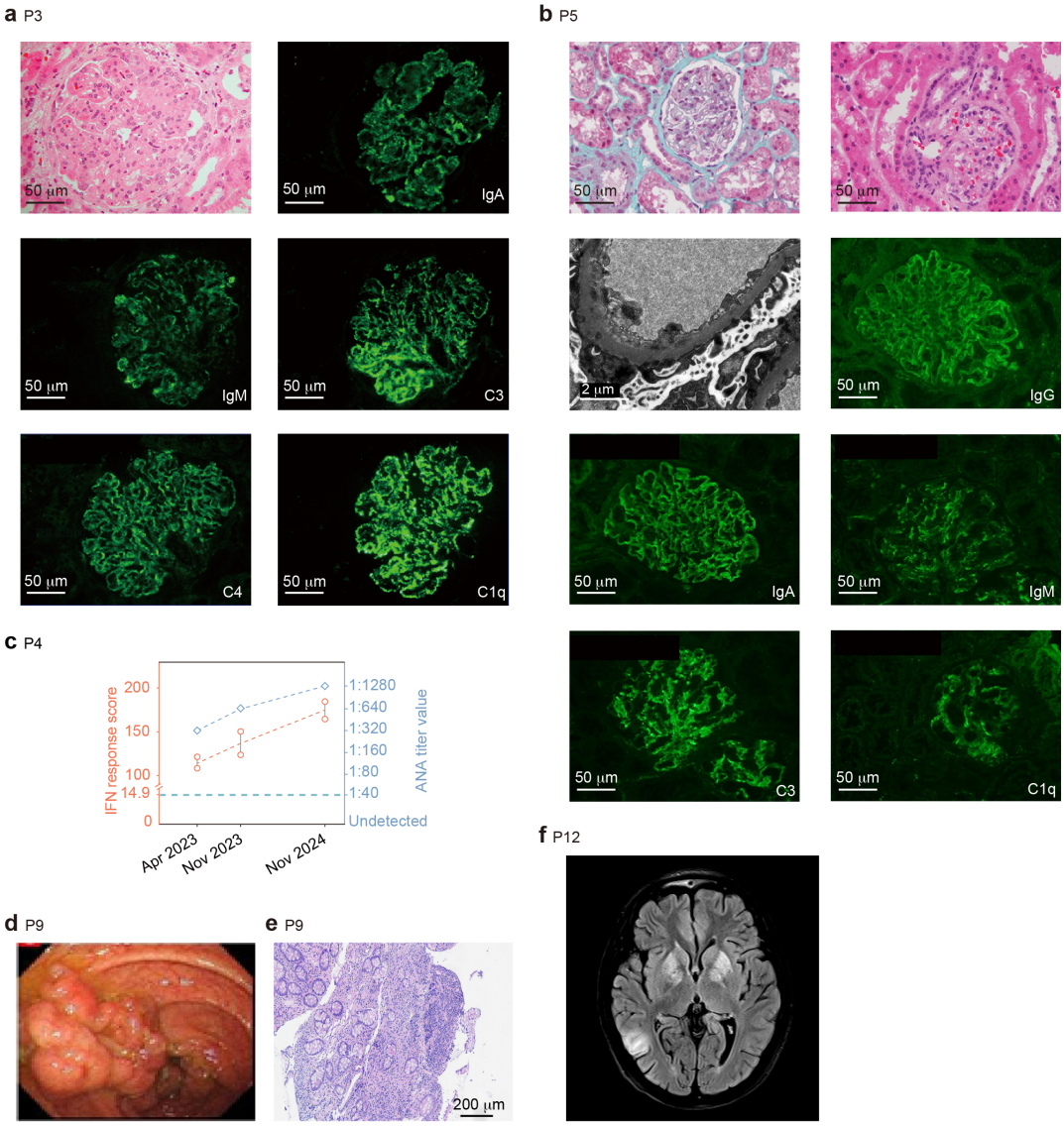

Supplementary Fig. 1 Additional clinical features of the patients.

a Representative renal histopathology images from P3. Hematoxylin and eosin (H&E) staining demonstrates neutrophil infiltration with mesangial and endocapillary proliferation (×400). Immunofluorescence (IF) reveals diffuse granular IgA, IgM, C3, C4, and C1q deposition in the capillary loops, respectively (×400). **b** Representative renal histopathology images from P5. Masson's trichrome staining demonstrates segmental eosinophilic deposits on the epithelial side (×400). H&E staining shows mesangial cell proliferation (×400). Electron microscopy reveals abundant tubuloreticular inclusions. IF shows diffuse IgG, IgA, IgM, C3, and C1q deposition,

respectively (×400). **c** Interferon (IFN) response scores and antinuclear (ANA) titers from P4 at three time points. **d** A colonoscopic image of the ileocecal region from P9, revealing finger- and coral-like inflammatory polyps. **e** A H&E-stained section of an ileocecal biopsy specimen from P9, revealing mucosal architectural distortion, crypt irregularities, chronic inflammation of the mucosal lining with interstitial edema, and inflammatory cell infiltration in the lamina propria. **f** An axial fluid-attenuated inversion recovery (FLAIR) image from P12, showing heterogeneous and markedly increased signal intensity in the bilateral basal ganglia, along with gyriform hyperintensity in the right frontal lobe and bilateral temporo-occipital lobes. The left lateral ventricle appeared slightly enlarged compared to the right.

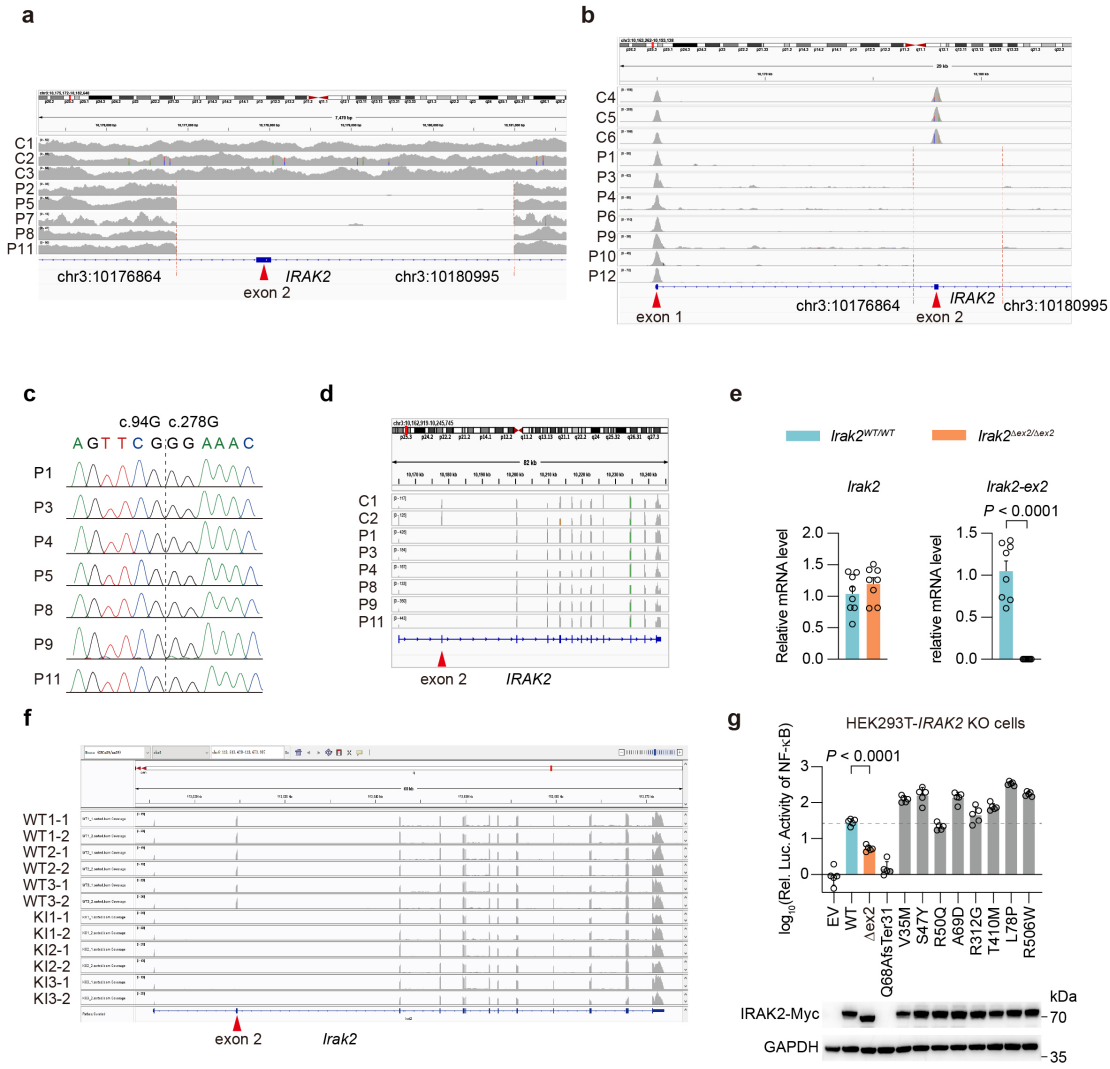

Supplementary Fig. 2 Identification of the *IRAK2*-Δ*ex2* mutation.

a Whole genome sequencing read coverage of *IRAK2* exon 2 in three unaffected controls and five patients (P2, P5, P7, P8, and P11) visualized by Integrative Genomics Viewer (IGV). **b** Whole exome sequencing read coverage of *IRAK2* in three unaffected controls and seven patients (P1, P3, P4, P6, P9, P10, and P12) visualized by IGV. **c** Sanger sequencing of complementary DNA (cDNA) from P1, P3, P4, P5, P8, P9, and P11. c.94G and c.278G flank the deleted exon 2 region in cDNA. **d** bulk RNA sequencing read coverage of *IRAK2* exon 2 in peripheral blood mononuclear cells (PBMCs) from P1, P3, P4, P8, P9, P11, and two unaffected controls, visualized using IGV. **e** Quantitative PCR of *Irak2* expression in bone marrow-derived macrophages (BMDMs), using primers outside (left) or inside (right) exon 2. Two-sided Student's *t*

test with Welch's correction was applied. Bars represent mean of *n* = 8 ± SEM (biological replicates). **f** bulk RNA sequencing read coverage of *Irak2* exon 2 in BMDMs visualized by IGV. **g** NF-κB luciferase reporter assay in HEK293T-*IRAK2* knockout (KO) cells overexpressing control empty vector (EV), IRAK2-WT, IRAK2-Δex2, or variants (Q68AfsTer31, V35M, S47Y, R50Q, A69D, R312G, T410M, L78P, and R506W). Cells were co-transfected with NF-κB-luciferase and renilla reporters and collected 24 hours post-transfection. One-way ANOVA with Dunnett's multiple-comparisons test was performed. Bars represent mean of *n* = 5 ± SEM (biological replicates).

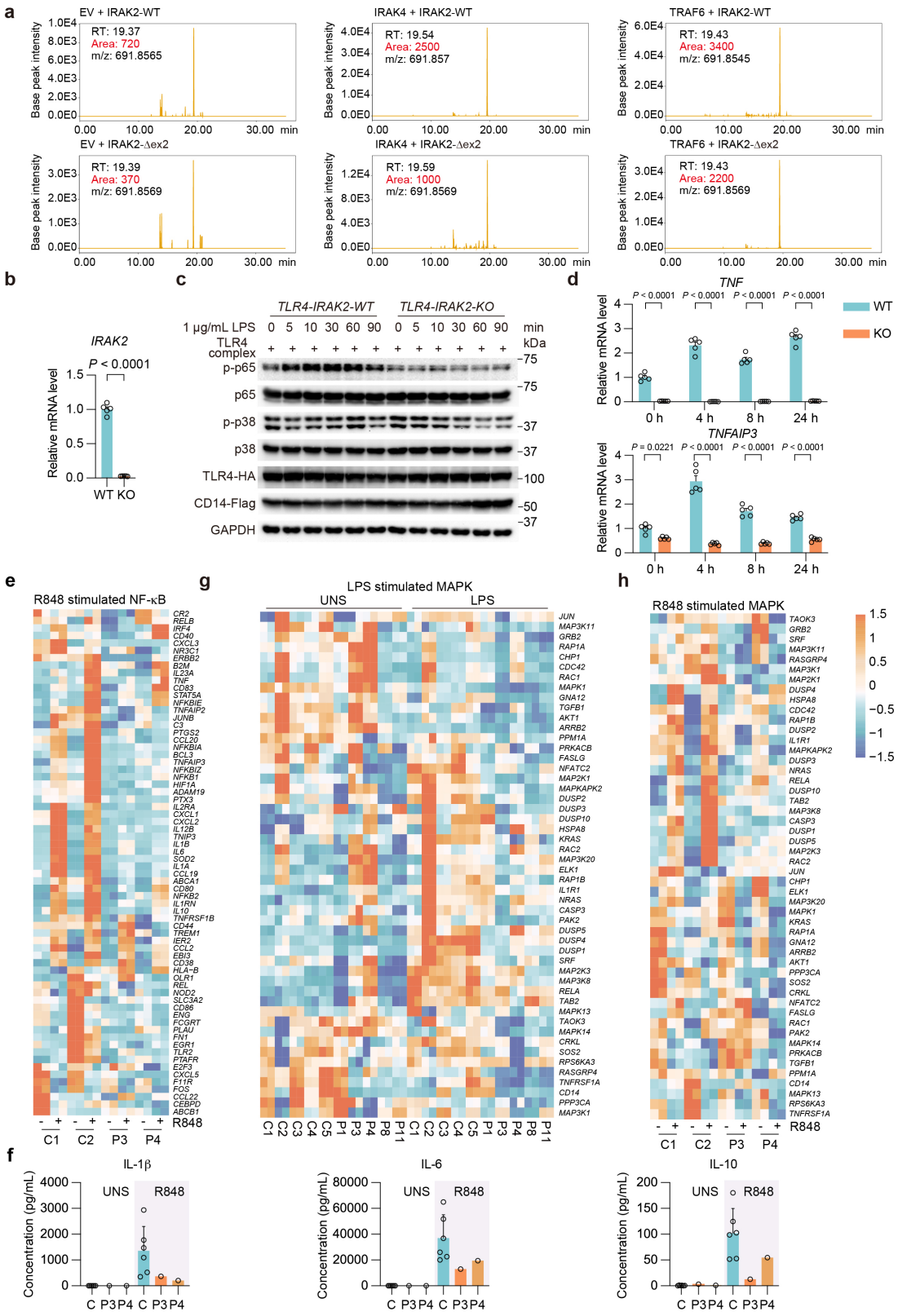

Supplementary Fig. 3 Defective NF-κB signaling via the Myddosome complex in DIRAK2.

a Representative extracted ion chromatograms of the IRAK2 peptide TSAAYLPEDFIR (m/z ≈ 691.856) in the co-immunoprecipitation eluates described in Fig. 2b. The retention time (RT), peak area, and m/z values are indicated in each panel. Normalized label-free quantification (LFQ) intensities for IRAK2 protein were 39049 (EV + IRAK2-WT), 19147 (EV + IRAK2-Δex2), 217080 (IRAK4 + IRAK2-WT), 64343 (IRAK4 + IRAK2-Δex2), 197950 (TRAF6 + IRAK2-WT), and 212700 (TRAF6 + IRAK2-Δex2). EV, empty vector; m/z, mass-to-charge ratio. **b** Quantitative PCR (qPCR) of *IRAK2* expression in HEK293T-*IRAK2* wild-type (WT) and knockout (KO) cells (TLR4+). Two-sided Student's *t* test with Welch's correction was applied. Bars represent mean of n = 5 ± SEM (biological replicates). **c** Immunoblotting of NF-κB and MAPK signaling in HEK293T-*IRAK2* WT and KO cells (TLR4+) after stimulation with 1 µg/mL LPS for indicated times. The experiment was repeated independently three times with similar results. **d** qPCR of NF-κB-related gene expression in HEK293T-*IRAK2* WT and KO cells (TLR4+) after stimulation with 100 ng/mL LPS for indicated times. Two-way ANOVA with Šídák's multiple-comparisons test was applied. Bars represent mean of n = 5 ± SEM (biological replicates). **e** RNA sequencing analysis of NF-κB pathway in peripheral blood mononuclear cells (PBMCs) from P3, P4, and two unaffected controls. Cells were treated with 1 µg/mL R848 (TLR7/8 agonist) or left unstimulated for 12 hours. Each sample was processed in two technical repeats. **f** Cytokine secretion in PBMCs from P3, P4, and six unaffected controls, treated as described in (**e**). Supernatants were analyzed using Cytometric Bead Array. Bars represent mean of n = 6 ± SEM (biological replicates). **g** RNA sequencing analysis of MAPK pathway in PBMCs from P1, P3, P4, P8, P11, and five unaffected controls. Cells were treated with 1 µg/mL LPS or left unstimulated for 12 hours. Each sample was processed in two technical repeats. **h** RNA sequencing analysis of MAPK pathway from samples described in (**e**).

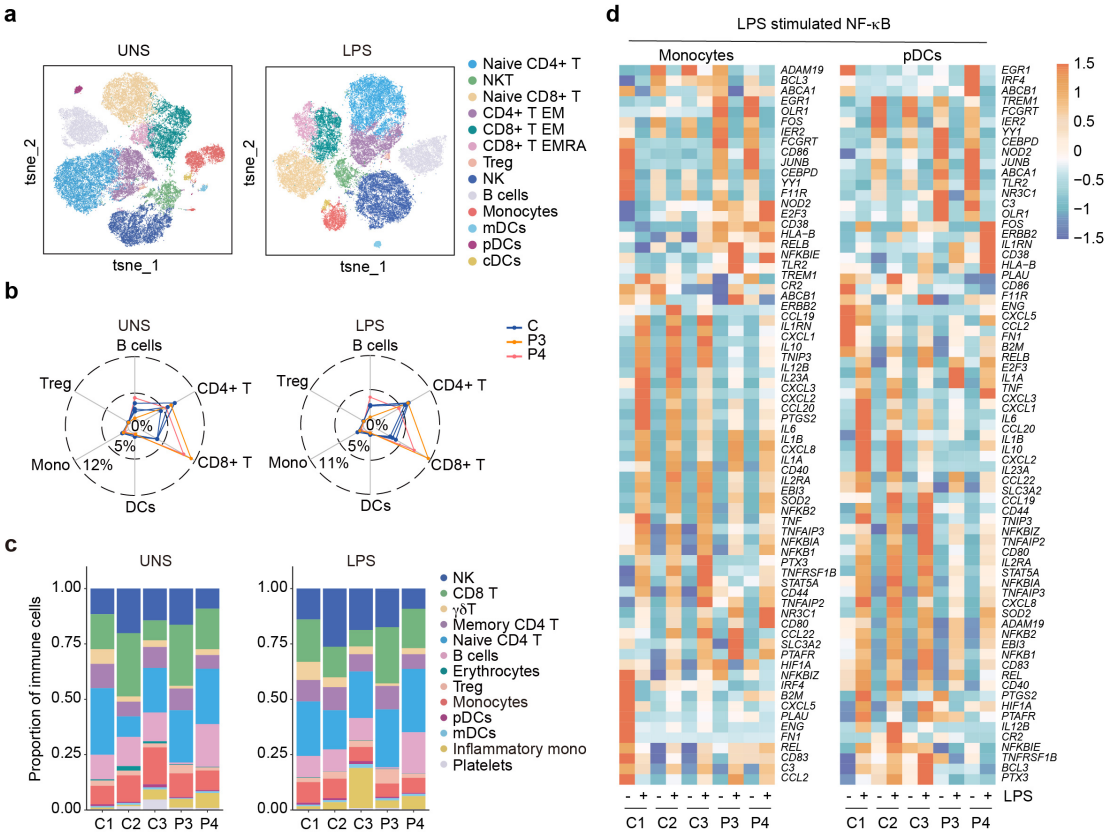

Supplementary Fig. 4 CyTOF and scRNA-seq define immune cell subset distributions.

a t-distributed stochastic neighbor embedding (t-SNE) plots of cytometry by time of flight (CyTOF) data, illustrating immunophenotyping of 5*10,000 $CD45^+$ $CD66b^-$ live peripheral blood mononuclear cells (PBMCs) from P3, P4, and three unaffected controls following LPS treatment (1 μg/mL, 12 hours) or left unstimulated (UNS). **b** Immune cell composition derived from CyTOF data described in (**a**) under UNS (left) and LPS-stimulated (right) conditions. **c** Immune cell composition derived from single-cell RNA sequencing (scRNA-seq) data (P3, P4, and three unaffected controls) under UNS (left) and LPS-stimulated (1 μg/mL, 8 hours) (right) conditions. **d** scRNA-seq of monocytes and plasmacytoid dendritic cells (pDCs) from samples described in (**c**), revealing defective NF-κB pathway activation in patients following LPS stimulation (1 μg/mL, 8 hours). mDCs denotes myeloid dendritic cells; cDCs denotes conventional dendritic cells.

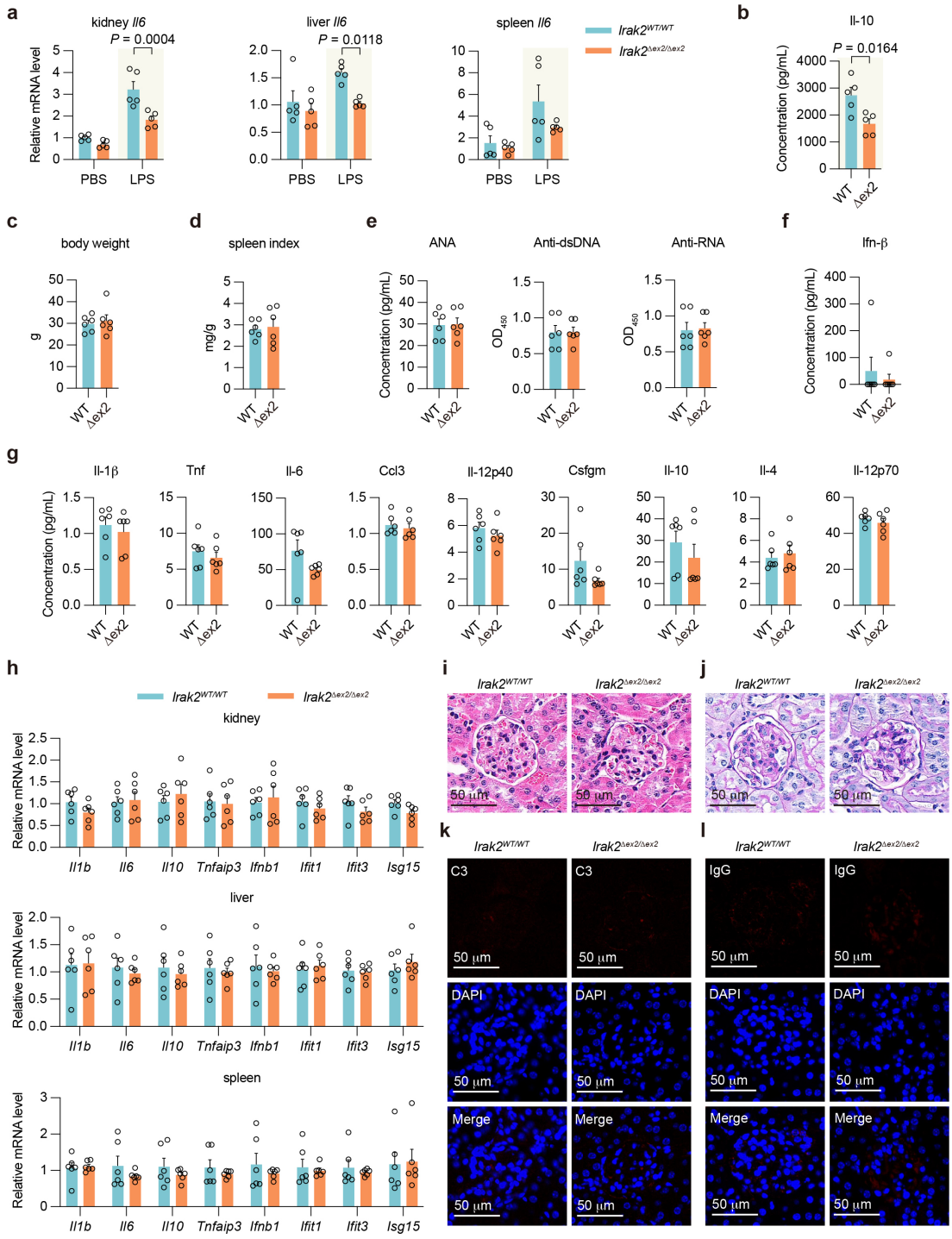

Supplementary Fig. 5 Baseline phenotyping of aged *Irak2*$^{\Delta ex2/\Delta ex2}$ and *Irak2*$^{WT/WT}$ mice reveals no spontaneous pathology.

a Tissue *Il6* expression in *Irak2*$^{\Delta ex2/\Delta ex2}$ and *Irak2*$^{WT/WT}$ mice 2 hours after intraperitoneal (i.p.) injection of LPS (10 mg/kg) or PBS, measured by quantitative PCR (qPCR). 10-

week-old seventh-generation female mice were used, with wild-type (WT) littermates as controls. Two-way ANOVA with Šídák's multiple-comparisons test was applied. Bars represent mean of n = 5 ± SEM (biological replicates). **b** Serum Il-10 levels from *Irak2*$^{\Delta ex2/\Delta ex2}$ and *Irak2*$^{WT/WT}$ mice 4 hours after i.p. injection of *E. coli* (5×10^8 CFU per mouse). 24-week-old sixth-generation female mice were used, with WT littermates as controls. Two-sided Student's t test with Welch's correction was applied. Bars represent mean of n = 5 ± SEM (biological replicates). **c**, **d** Body weight (**c**) and spleen index (**d**) at baseline in *Irak2*$^{\Delta ex2/\Delta ex2}$ and *Irak2*$^{WT/WT}$ mice. 50-week-old fifth-generation female mice were used, with WT littermates as controls. Two-sided Student's t test with Welch's correction was applied. Bars represent mean of n = 6 ± SEM (biological replicates). **e** Autoantibody profiling of mice described in (**c**, **d**). Two-sided Student's t test with Welch's correction was applied. Bars represent mean of n = 6 ± SEM (biological replicates). OD_{450}, optical density at 450 nm. **f**, **g** Serum Ifn-β (**f**) and inflammatory cytokines/chemokines (**g**) in mice described in (**c**, **d**). Two-sided Student's t test with Welch's correction was applied. Bars represent mean of n = 6 ± SEM (biological replicates). **h** Tissue qPCR analysis of NF-κB and type I IFN pathways in mice described in (**c**, **d**). Two-way ANOVA with Šídák's multiple-comparisons test was applied. Bars represent mean of n = 6 ± SEM (biological replicates). **i**, **j** Renal histology from mice in (**c**, **d**) (n = 6, biological replicates). Hematoxylin and eosin (**i**) and Periodic acid–Schiff (**j**) staining. **k**, **l** Renal immunofluorescence staining for C3 (**k**) and IgG (**l**) in mice described in (**c**, **d**) (n = 6, biological replicates).

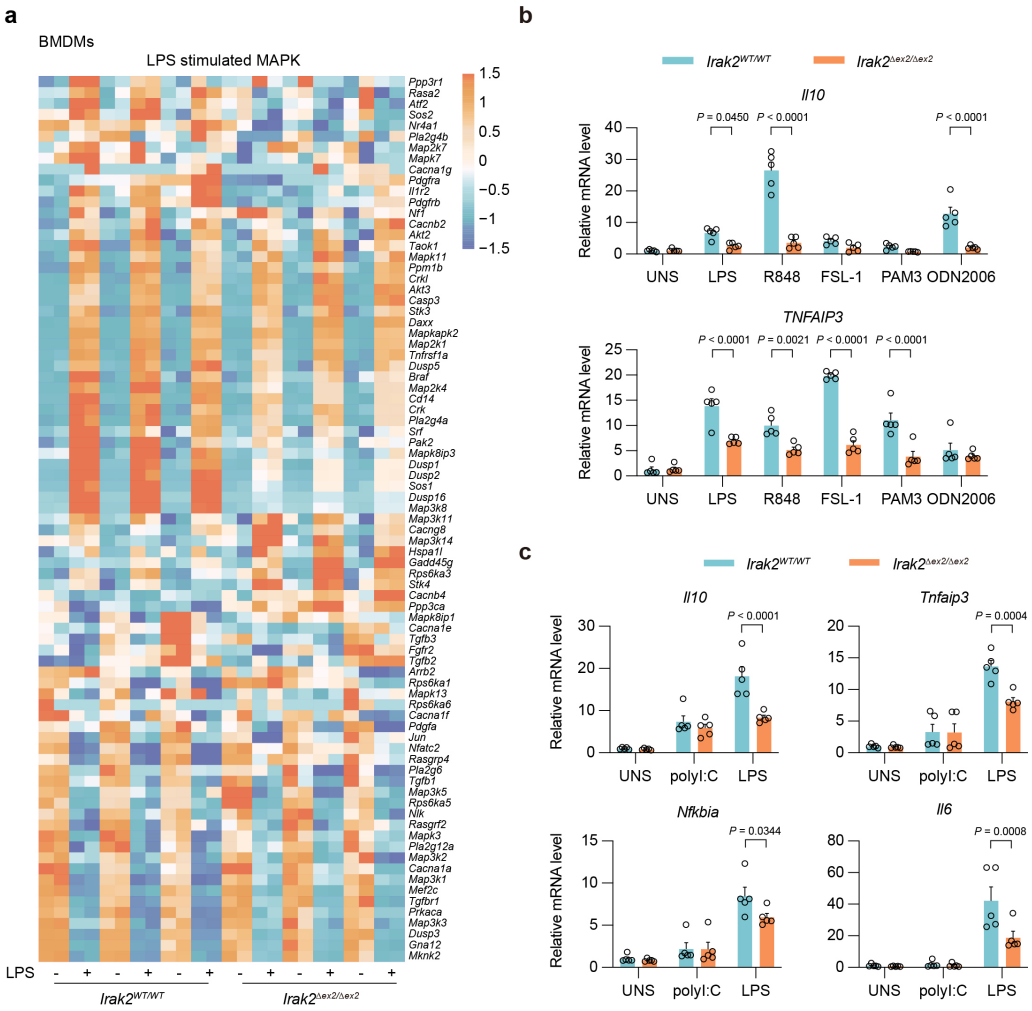

Supplementary Fig. 6 *Irak2-Δex2* leads to multiple impaired TLRs signaling in BMDMs.

a RNA sequencing analysis of MAPK pathway in bone marrow-derived macrophages (BMDMs) treated with 100 ng/mL LPS or left untreated for 8 hours (n = 3, biological replicates). Each sample was processed in two technical repeats. **b** Quantitative PCR (qPCR) of NF-κB-related gene expression in BMDMs treated with 100 ng/mL LPS, 25 ng/mL R848, 50 ng/mL FSL-1, 1 µg/mL Pam_3Cys-Ser-$(Lys)_4$ (PAM3), 2 µM ODN2006, or left unstimulated (UNS) for 8 hours. BMDMs were isolated from 12-week-old fifth-generation female littermate mice. Two-way ANOVA with Šídák's multiple-comparisons test was applied. Bars represent mean of n = 5 ± SEM (biological replicates). **c** qPCR of NF-κB-related gene expression in BMDMs treated with 100 ng/mL LPS, 5 µg/mL poly(I:C), or left UNS for 4 hours. BMDMs were isolated from 10-

week-old seventh-generation female littermate mice. Two-way ANOVA with Šídák's multiple-comparisons test was applied. Bars represent mean of $n = 5 \pm$ SEM (biological replicates).

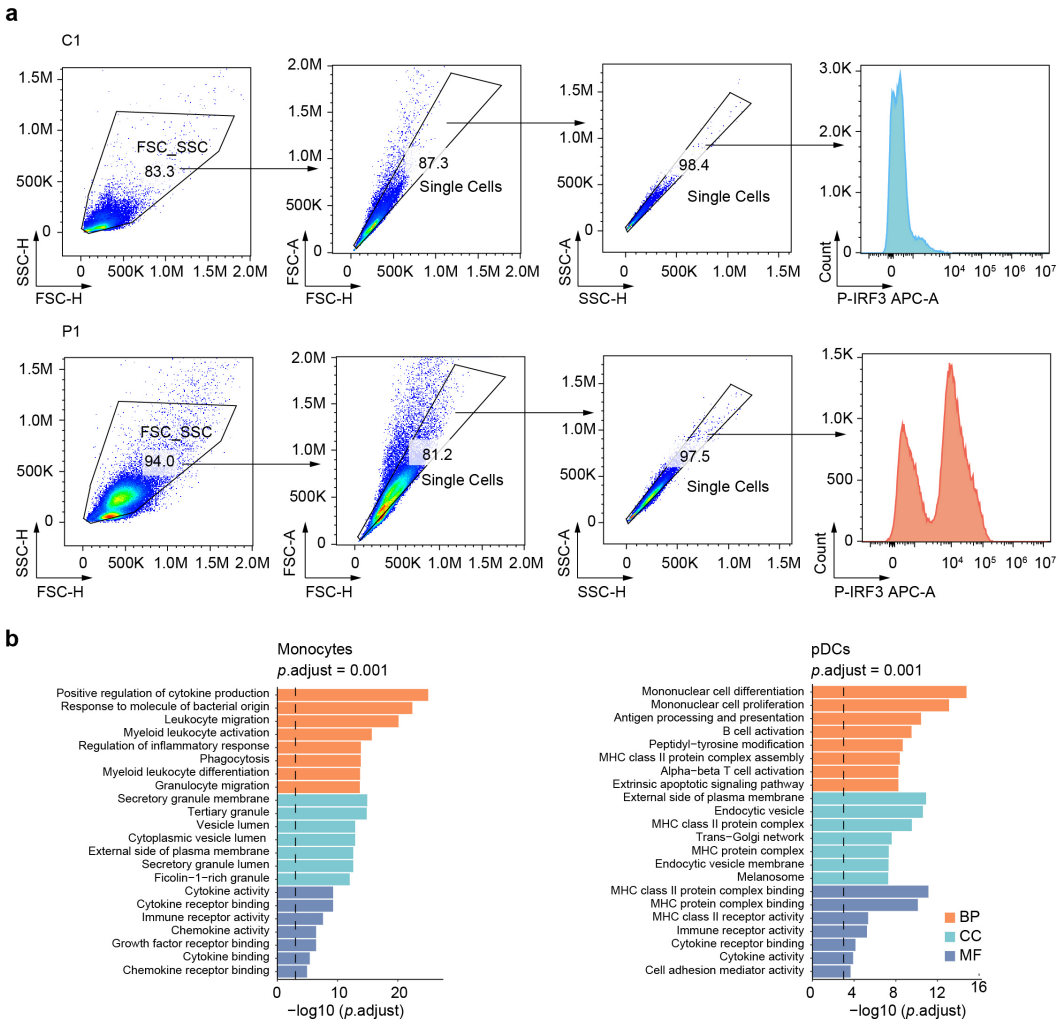

Supplementary Fig. 7 Flow cytometry gating strategy and aberrantly activated inflammatory responses in patient-derived cells.

a Representative flow cytometry gating strategy for Fig. 4b, showing one unaffected control (C1) and one patient (P1). Peripheral blood mononuclear cells (PBMCs) were gated by FSC/SSC and singlet discrimination, followed by analysis of phosphorylated IRF3 (p-IRF3) expression. Numbers indicate the percentage of cells within the parent gate. **b** Functional enrichment analysis (single-cell RNA sequencing) of monocytes and plasmacytoid dendritic cells (pDCs) from P3, P4, and three unaffected controls following LPS stimulation (1 μg/mL, 8 hours) based on Gene Ontology categories: Biological Process (BP), Cellular Component (CC), and Molecular Function (MF). *P* values were adjusted using the Benjamini-Hochberg method.

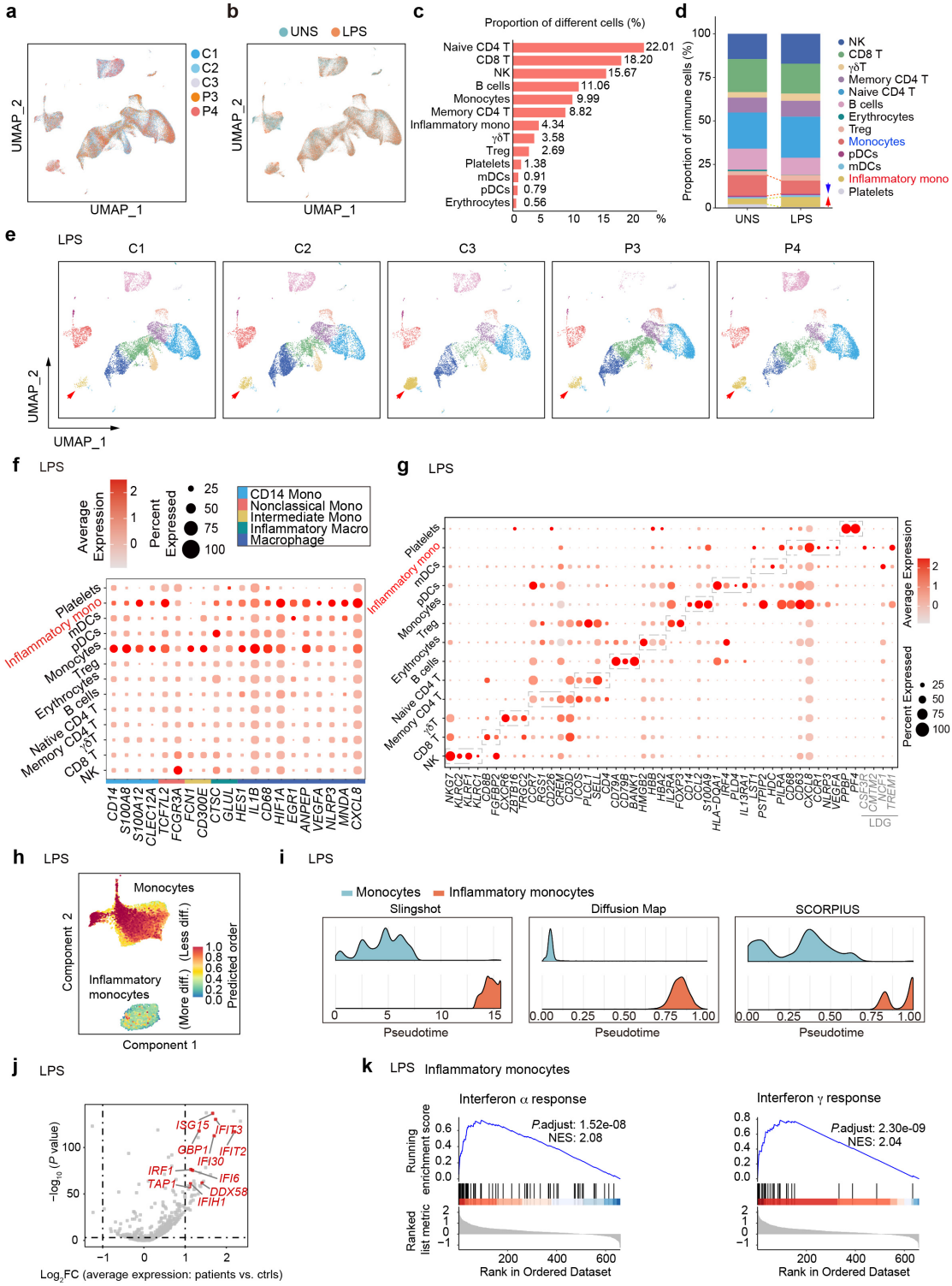

Supplementary Fig. 8 Elevated type I interferon signature detected by scRNA-seq.

a, **b** Uniform distribution of 104,028 cells across samples, colored by individual (**a**) or treatment condition (**b**). **c** Relative proportions of the 13 annotated peripheral blood

mononuclear cells (PBMCs) subsets, all within expected physiological ranges. **d** Changes in cell type proportions under unstimulated (UNS) and LPS-stimulated conditions. A reduced proportion of monocytes and an increased proportion of inflammatory monocytes were observed in all samples following LPS stimulation (1 μg/mL, 8 hours). **e** Uniform manifold approximation and projection (UMAP) plots of the 13 cell subsets shown individually by sample under LPS-stimulated conditions. Inflammatory monocytes were observed in both patients (P3, *n* = 9345 cells; P4, *n* = 8941 cells) and three unaffected controls (C1, *n* = 10019 cells; C2, *n* = 10135 cells; C3, *n* = 8941 cells), indicated by red arrowheads. **f**, **g** Bubble plots of marker gene expression used to define monocytes and inflammatory monocytes following LPS stimulation (1 μg/mL, 8 hours). Marker genes associated with the myeloid cell lineage, including *CD14*, *S100A8*, *HES1*, *IL1B*, *CD68*, *HIF1A*, *EGR1*, *ANPEP*, *VEGFA*, *NLRP3*, *MNDA*, and *CXCL8*[5-13], were highly expressed in the inflammatory monocytes. Bubble size represents the percentage of expressing cells; color indicates average expression. LDG, low-density granulocytes. **h** Predicted differentiation states of monocytes and inflammatory monocytes assessed by CytoTRACE following LPS stimulation. Inflammatory monocytes (*n* = 34437 cells) exhibited lower CytoTRACE scores than monocytes (*n* = 2580 cells), indicating a more differentiated state. **i** Pseudotime trajectory analyses of monocytes and inflammatory monocytes following LPS stimulation, computed using three algorithms. A rightward shift in pseudotime indicates a more advanced differentiation trajectory. **j** Volcano plot of differentially expressed genes in inflammatory monocytes from P3/P4 compared with unaffected controls following LPS stimulation (1 μg/mL, 8 hours). **k** Gene set enrichment analysis plots of enriched pathways in inflammatory monocytes of P3/P4 versus unaffected controls following LPS stimulation (1 μg/mL, 8 hours).

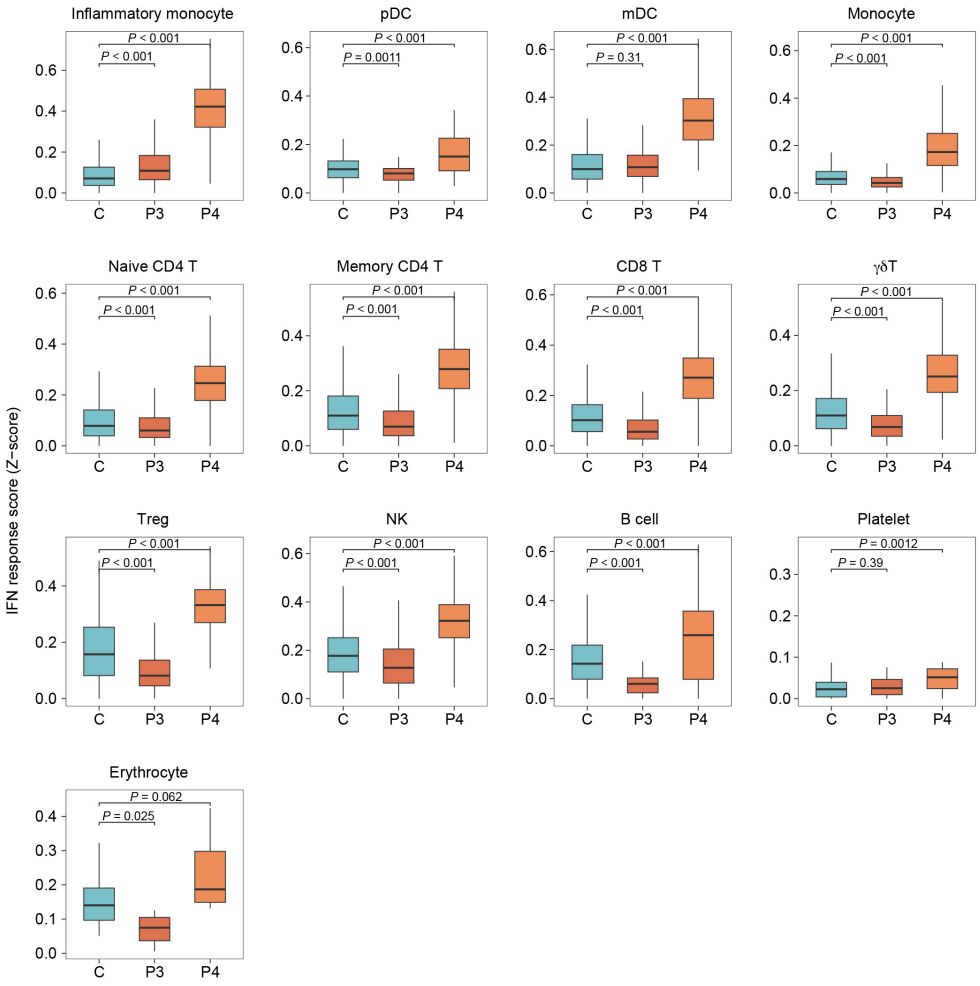

Supplementary Fig. 9 Type I interferon response scores across cell types by scRNA-seq.

Type I interferon (IFN) response scores across cell types following LPS stimulation, calculated from single-cell RNA sequencing data. Boxplots represent the median and interquartile range, and the whiskers denote minimum and maximum values. The two-sided Wilcoxon rank-sum test was performed.

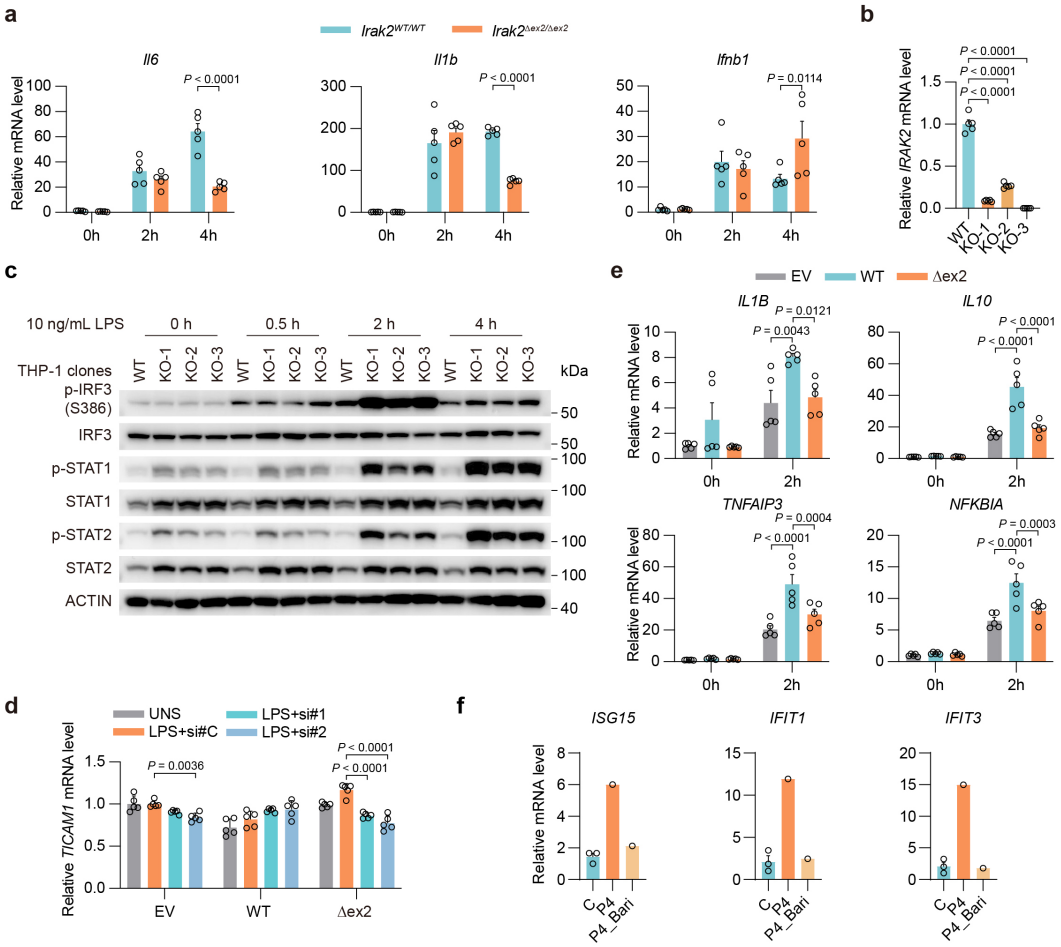

Supplementary Fig. 10 Elevated type I interferon signature in BMDMs and THP-1, and effect of JAK inhibitor treatment in PBMCs and THP-1.

a Quantitative PCR (qPCR) of *Il6*, *Il1b*, *Ifnb1* expression in bone marrow-derived macrophages (BMDMs) treated with 100 ng/mL LPS for 0, 2, or 4 hours. BMDMs were isolated from 12-week-old fifth-generation female littermate mice. Two-way ANOVA with Šídák's multiple-comparisons test was applied. Bars represent mean of *n* = 5 ± SEM (biological replicates). **b** qPCR of *IRAK2* expression in PMA-differentiated THP-1 *IRAK2* knockout (KO) and wild-type (WT) cells. One-way ANOVA with Dunnett's multiple-comparisons test was performed. Bars represent mean of *n* = 5 ± SEM (biological replicates). PMA, phorbol 12-myristate 13-acetate. **c** Immunoblotting of IRF3, STAT1, and STAT2 phosphorylation in PMA-differentiated THP-1 *IRAK2* KO and WT cells following LPS stimulation (10 ng/mL) for indicated times. The experiment was repeated independently three times with similar results. **d** qPCR of *TICAM1* expression

in reconstituted THP-1 cells following LPS stimulation (10 ng/mL, 2 hours). *TICAM1* (TRIF) was knocked down using two independent siRNAs (siRNA#1 and siRNA#2), with a non-targeting siRNA (siRNA#C) as control. Two-way ANOVA with Tukey's multiple-comparisons test was applied. Bars represent mean of $n = 5$ ± SEM (biological replicates). **e** qPCR of NF-κB-related gene expression in *IRAK2* KO THP-1 cells reconstituted with control empty vector (EV), IRAK2-WT, or IRAK2-Δex2, stimulated with 10 ng/mL LPS for 0 or 2 hours. Two-way ANOVA with Tukey's multiple-comparisons test was applied. Bars represent mean of $n = 5$ ± SEM (biological replicates). **f** qPCR validation of *ISG15*, *IFIT1*, and *IFIT3* expression in peripheral blood mononuclear cells from P4 and three unaffected controls described in Fig. 5i. P4_Bari indicates Baricitinib-treated PBMCs (0.5 μM, 12 hours). Bars represent mean of $n = 3$ ± SEM (biological replicates).

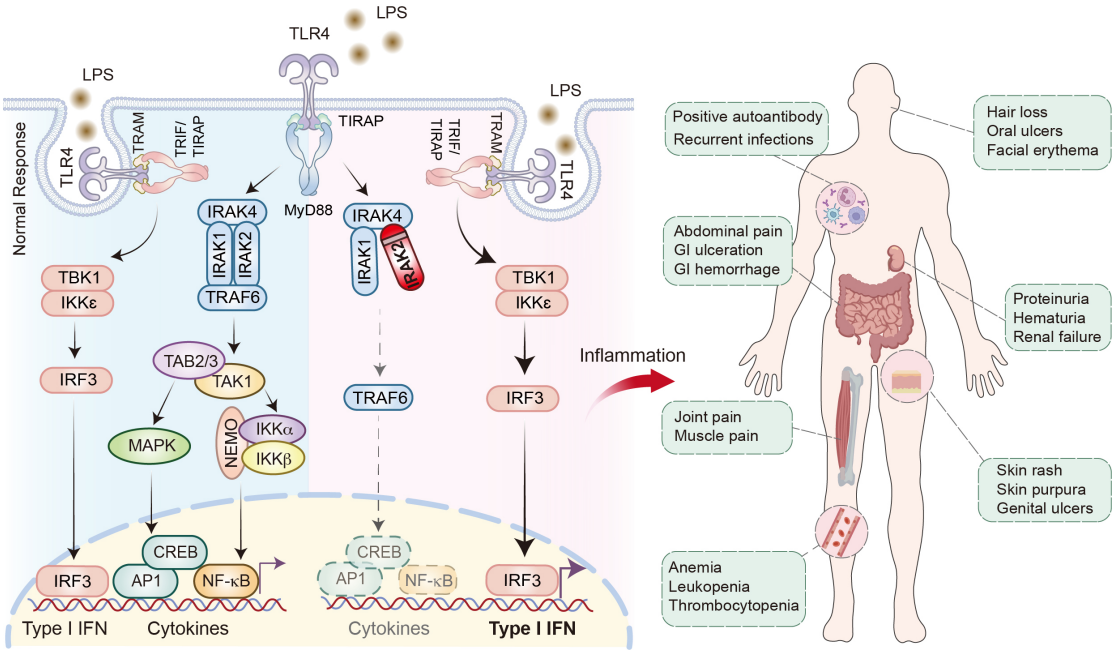

Supplementary Fig. 11 Schematic overview of a hypothetical DIRAK2 mechanism and clinical spectrum.

Supplementary Tables

Supplementary Table 1 Clinical features of the patients

Patients	P1	P2	P3	P4	P5	P6
Age at onset	1 month	49 years	22 years	22 years	13 years	10 years
Sex	Female	Female	Female	Female	Female	Female
Symptoms of initial presentation	Cough and expectoration	Joint pain, recurrent fever, and cough	Facial erythema, edema, and thrombocytopenia	Hair loss and waist area skin rashes	Purpura, swelling of limbs, and joints pain	Fatigue and hair loss
Infections	Pneumonia; Otitis media; Sinusitis	Cytomegalovirus infection; Pneumonia	Viral warts; Severe COVID-19 pneumonia			Herpes zoster; Pneumonia
Musculoskeletal manifestations	Hypotonia and weakness in early infancy	Joints pain	Joints pain		Muscle and joints pain	Muscle and joints pain
Cutaneous and mucosal manifestations			Butterfly facial erythema; Hair loss	Rash (waist area); Hair loss	Purpura	Butterfly facial erythema; Hair loss; Rash (back area)
Gastrointestinal manifestations						Anorexia
Hematologic manifestations			Anemia; Thrombocytopenia		Anemia; Leukopenia; Thrombocytopenia	Anemia
Urogenital manifestations			Hematuria; Proteinuria; Renal failure		Hematuria; Proteinuria; Renal failure	Hematuria; Proteinuria
Neurological manifestations	Delayed mental and intellectual development					
Current and past treatment	Antibiotics; IVIG	Antibiotics; Glucocorticoids; IVIG	Glucocorticoids; HCQ; CTX MMF/AZA; Tacrolimus; Belimumab		Glucocorticoids; HCQ; MMF; Tacrolimus; Belimumab	Glucocorticoids; HCQ; MMF; Telitacicept
Diagnosis	PID	PID	SLE; LN		SLE; LN	SLE; LN

Patients	P7	P8	P9	P10	P11	P12
Age at onset	51 years	6 years	14 years	4 years	20 years	14 years
Sex	Male	Male	Male	Female	Male	Female
Symptoms of initial presentation	Recurrent epistaxis	Abdominal pain, vomiting, and bloody stool	Recurrent fever, abdominal pain, and oral/genital ulcers	Joints pain and recurrent oral ulcers	Goiter	Syncope
Infections	Bacterial pneumonia			Left sphenoid sinusitis		Bilateral mastoiditis; Left ethmoid sinusitis
Musculoskeletal manifestations	Joints pain		Osteoporosis	Joints pain; Joint effusion		
Cutaneous and mucosal manifestations	Skin purpura; Oral ulcers		Rash (back area); Oral ulcers; Genital ulcers	Oral ulcers; Rash	Lichen planus	
Gastrointestinal manifestations		Abdominal pain; Vomiting; Gastrointestinal hemorrhage	Abdominal pain; Intestinal obstruction; Perianal abscess	Abdominal pain		
Hematologic manifestations	Anemia; Thrombocytopenia	Anemia	Anemia			
Urogenital manifestations	Hematuria; Proteinuria; Renal failure		Proteinuria			
Neurological manifestations						Impaired memory; Slow mental responses
Current and past treatment	Glucocorticoids; Sirolimus	Glucocorticoid; Infliximab; AZA	Glucocorticoids; CTX; AZA; Vitamin D	Glucocorticoids; NSAIDs; MTX; Vitamin D		Glucocorticoids; Mecobalamin; Vitamin B6
Diagnosis	SLE; LN	IBD	BD	JIA	Hashimoto's thyroiditis	Autoimmune encephalitis

Abbreviations: IVIG, Intravenous immunoglobulin; HCQ, Hydroxychloroquine; CTX, Cyclophosphamide; MMF, Mycophenolate mofetil; AZA, Azathioprine; NSAIDs, Nonsteroidal anti-inflammatory drugs; MTX, Methotrexate; PID, Primary immunodeficiency; SLE, Systemic lupus erythematosus; LN, Lupus nephritis; IBD, Inflammatory bowel disease; JIA, Juvenile idiopathic arthritis; BD, Behçet's disease.

Supplementary Table 2 The pathogens of the patients diagnosed with primary immunodeficiency

Patients	P1	P2
Gram-positive bacteria		
Streptococcus pneumoniae	+	
Streptococcus constellatus	+	
Gram-negative bacteria		
Klebsiella pneumoniae	+	
Fusobacterium nucleatum	+	
Haemophilus influenzae	+	
Pseudomonas maltophilia		+
Pseudomonas aeruginosa		+
Fungus		
Aspergillus	+	
Pneumocystis jirovecii		+
Candida albicans		+
Virus		
Rhinovirus	+	
Cytomegalovirus		+

Supplementary Table 3 Laboratory features

Patients	P1	P2	P3	P4	P5	P6	P7	P8	P9	P10	P11	P12
White blood cell (4-10 ×10^9 cells/L)	6.87	3.33	7.3	5.57	4.63	3.62	3.79	19.9	10.94	6.4	4.4	11.39
Hemoglobin (120-175 g/L)	125	64	95	150	84	81	101	45	115	132	160	123
Platelet (100-300×10^9 cells/L)	305	209	146	190	5.4	150	38	444	431	256	229	369
CRP (0-8 mg/L)	4.1	136	<0.5	<0.5	<0.5	1.87	10.3	19.7	104	<0.5	NA	26.67
ESR (0-20 mm/h)	33	9	NA	NA	20	2	65	2	45	2	NA	NA
Albumin (40.0-55.0 g/L)	40.6	22.8	28.9	48.4	34	41.6	31.7	31.6	NA	44.2	49	47.2
Alanine transaminase (<50 U/L)	<10	54	25	20	11	24.5	37.4	4	8	17	33	12.5
Glutamic oxalic transaminase (<40 U/L)	16	62	13	17	13	46.6	37	12.3	10	25	31	25.2
Serum creatinine (μmol/L)	38	40	147	62	34.6	45	234	30	NA	38.5	87	53.8
Blood urea nitrogen (mmol/L)	4.2	5.2	9	4.49	3.8	6.08	11.27	5.8	NA	5.46	4.7	4.12
Immunoglobulin and complement												
IgG (7.51-15.6 g/L)	14.6	2.23	5.13	NA	16.4	25.3	NA	8.99	6.41	7.78	NA	NA
IgA (0.82-4.53 g/L)	1.77	0.103	3.82	NA	2.61	2.18	NA	2.3	NA	0.91	NA	NA
IgM (0.46-3.04 g/L)	0.77	0.053	0.34	NA	0.714	1.25	NA	0.79	NA	1.55	NA	NA
IgE (<200 U/L)	157.7	NA	59.3	NA	370	235	NA	8.4	NA	5.08	NA	NA
C3 (0.8-1.8 g/L)	1.08	NA	0.526	0.8	0.206	0.2	0.15	0.97	1.23	0.86	NA	NA
C4 (0.1-0.4 g/L)	0.23	NA	0.117	0.108	0.073	0.07	0.08	0.22	0.25	0.08	NA	NA
Auto-antibodies												
ANA	negative	negative	1:320	1:160	1:160	1:320	1:320	negative	negative	negative	negative	negative
dsDNA	negative	negative	negative	negative	positive	positive	positive	negative	negative	negative	negative	negative
Other positive auto-antibodies	negative	negative	Anti- Sm, RNP, SSA	ACL, A-β2-GP1	SSA, Ro52, SSB, A Jo-1, A-CenpB, A-RPA	Sm, SSA, RNP	APL	negative	negative	negative	Anti-TG, anti-TPO	negative

Abbreviations: CRP, C-reactive protein; ESR, Erythrocyte sedimentation rate; NA, Not available; ANA, Antinuclear antibody; ACL, Anti-cardiolipin; APL, Antiphospholipid; A-β2-GP1, Anti-β2 glycoprotein I; RNP, Ribonucleoprotein; SSA, Sjögren's syndrome-related antigen A; TG, Thyroglobulin; TPO, Thyroid peroxidase.

Supplementary Table 4 Clinical and immunological comparison of IRAK2, IRAK4, MyD88 and TLR4 deficiencies

	IRAK2 deficiency	IRAK4 deficiency	MyD88 deficiency	TLR4 deficiency
Hereditary Pattern	Autosomal recessive	Autosomal recessive	Autosomal recessive	Autosomal recessive
Age at Onset	1 month (youngest) and 51 years (oldest)	Most patients develop before 2 years old[14]	Most patients develop before 2 years old[15]	11 years old, 22 years old[16]
Sites of Infection	Noninvasive infection: respiratory tract, paranasal sinuses, otic system (middle/external ear and ear canal), gastrointestinal tract, skin/mucosa	Invasive infection: meningitis, sepsis, arthritis, osteomyelitis, deep inner organs/tissues abscesses[14]; Noninvasive infection: skin, upper respiratory tract, umbilical, lymph nodes[17]	Invasive infection: meningitis, sepsis, arthritis, osteomyelitis, deep inner organs/tissues abscesses[14]; Noninvasive infection: skin, upper respiratory tract, lymph nodes, gingiva/periodontium[17]	Perianal skin, ileocecal region[16]
Pathogens	*Streptococcus pneumoniae*, *Streptococcus constellatus*, *Klebsiella pneumoniae*, *Fusobacterium nucleatum*, *Haemophilus influenzae*, *Pseudomonas maltophilia*, *Pseudomonas aeruginosa*, *Aspergillus*, *Pneumocystis jirovecii*, *Candida albicans*, *Rhinovirus*, *Cytomegalovirus*	*Streptococcus pneumoniae*, *Staphylococcus aureus*, *Pseudomonas aeruginosa*, *Streptococcus species*, *Shigella sonnei*, *Neisseria meningitidis*, *Haemophilus influenzae type b*, *Clostridium septicum*[17]	*Streptococcus pneumoniae*, *Staphylococcus aureus*, *Pseudomonas aeruginosa*, *β-hemolytic Streptococci*, *Salmonella enteritidis*, *Haemophilus influenzae type e*, *Moraxella catarrhalis*[17]	*Escherichia coli*, *Gram-negative bacilli*[16]
Cytokine Profiles (*ex vivo* TLR/IL_1R Stimulation)	Reduced cytokine (IL-6, IL-1β, IL-10) response to TLR4 and TLR7/8 agonists	Reduced cytokine (IL-6, TNF) response to TLR1, 2, 4, 5, 6, 9 and IL-1R agonists[18]	Reduced cytokine (IL-6, IL-8, IL-1β, IL-10, IL-12) response to TLR1, 2, 4, 5, 6, 7, 8 and IL-1R agonists[19]	Reduced cytokine (IL-6, IL-8, TNF, IL-1α) response to TLR4 agonist, normal cytokine response to TLR2 agonist[16]
IFN Signature	Elevated serum IFN-β levels, increased baseline IRF3 phosphorylation in PBMCs, or upregulated ISGs expressions in some patients	Loss of IFN-γ upon IL-12, IL-1β, IL-18 stimulation[18]	Loss of IFN-β/IFN-λ upon IL-1β stimulation[19]	NA
Autoinflammatory Manifestations	Some patients with ESR (↑) and CRP (↑); Recurrent febrile episodes; Gastrointestinal, oral/genital ulcers; Non-pruritic rashes; Juvenile idiopathic arthritis; Macrophage activation syndrome	Poor inflammatory response[18]; Temperature: neonates (↓/-), infants (↓/-), children (↓/-); CRP: neonates (↑), infants (↓/-), children (↓/-); Pus formation[17]; Recurrent episodes of fever, Severe hypochromic microcytic, massive splenomegaly[20]; Neuroinflammation[20]; Juvenile idiopathic arthritis[21]	Poor inflammatory response[19]; Temperature: neonates (↓/-), infants (↓/-), children (↓/-); CRP: neonates (↓/-), infants (↓/-), children (↓/-); Pus formation[17]	Recurrent fever; Inflammatory bowel disease[16]
Autoimmune Manifestations	Systemic lupus erythematosus; Hashimoto's thyroiditis; Autoimmune encephalitis	Autoimmune encephalitis[22]	NA	NA

Abbreviations: CRP, C-reactive protein; ESR, Erythrocyte sedimentation rate; "-", normal; "↓", decrease; "↑", increase; ISGs, Interferon-stimulated genes; NA, Not available.

Supplementary Table 5 Antibodies used for mass cytometry analysis

Mass and Tag	Marker	Clone	Staining
89Y	CD45	HI30	Surface
115In	CD3	UCHT1	Surface
141Pr	CD62L	DREG-56	Surface
142Nd	TCRγ/δ	5A6.E9	Surface
143Nd	CD1c	L161	Surface
144Nd	CXCL10 (IP-10)	J034D6	Intra
145Nd	CD27	O323	Surface
146Nd	TNF-α	MAb11	Intra
147Sm	CD20	2H7	Surface
148Nd	CD19	HIB19	Surface
149Sm	CD25 (IL-2Rα)	24212	Surface
150Nd	CD11c	Bu15	Surface
151Eu	CD38	HIT2	Surface
152Sm	CD45RA	HI100	Surface
153Eu	CD123 (IL-3Rα)	6H6	Surface
154Sm	CD197 (CCR7)	G043H7	Surface
155Gd	CD15 (SSEA-1)	W6D3	Surface
156Gd	IL-6	MQ2-13A5	Intra
157Gd	IL-4	MP4-25D2	Intra
158Gd	STAT3 Phospho (Tyr705)	13A3-1	Intra
159Tb	CD56	NCAM16.2	Surface
160Gd	IL-8	E8N1	Intra
161Dy	IL-17A	BL168	Intra
162Dy	IL-1β (IL-1F2)	8516	Intra
163Dy	IL-2	MQ1-17H12	Intra
164Dy	CD141 (Thrombomodulin)	M80	Surface
165Ho	IFN-γ	B27	Intra
166Er	IL-23 (p19)	HLT2736	Intra
167Er	STAT1 Phospho (Ser727)	A15158B	Intra
168Er	GM-CSF	BVD2-21C11	Intra
169Tm	CD33	WM53	Surface
170Er	CD66b	G10F5	Surface
171Yb	CD127 (IL-7Rα)	A019D5	Surface
172Yb	HLA-DR	L243	Surface
173Yb	IL-10	JES3-9D7	Intra
174Yb	CD14	M5E2	Surface
175Lu	CD16	3G8	Surface
176Yb	Interferon α (IFN-α)	144BS	Intra
197Au	CD4	RPA-T4	Surface
198Pt	CD8a	RPA-T8	Surface
209Bi	CD11b	M1/70	Surface

Supplementary References

1. Aringer, M. *et al.* 2019 European League Against Rheumatism/American College of Rheumatology classification criteria for systemic lupus erythematosus. *Ann Rheum Dis* **78**, 1151-1159 (2019).
2. Postal, M. *et al.* Type I interferon in the pathogenesis of systemic lupus erythematosus. *Curr Opin Immunol* **67**, 87-94 (2020).
3. Xiong, H. *et al.* Cytotoxic CD161(-)CD8(+) T(EMRA) cells contribute to the pathogenesis of systemic lupus erythematosus. *EBioMedicine* **90**, 104507 (2023).
4. Agamia, N. *et al.* Interferon-gamma serum level and immunohistochemical expression of CD8 cells in tissue biopsies in patients with alopecia areata in correlation with trichoscopic findings. *Dermatol Ther* **33**, e13718 (2020).
5. Guilliams, M. *et al.* Dendritic cells, monocytes and macrophages: a unified nomenclature based on ontogeny. *Nat Rev Immunol* **14**, 571-8 (2014).
6. MacParland, S.A. *et al.* Single cell RNA sequencing of human liver reveals distinct intrahepatic macrophage populations. *Nat Commun* **9**, 4383 (2018).
7. Martin, J.C. *et al.* Single-Cell Analysis of Crohn's Disease Lesions Identifies a Pathogenic Cellular Module Associated with Resistance to Anti-TNF Therapy. *Cell* **178**, 1493-1508 e20 (2019).
8. Roquilly, A., Mintern, J.D. & Villadangos, J.A. Spatiotemporal Adaptations of Macrophage and Dendritic Cell Development and Function. *Annu Rev Immunol* **40**, 525-557 (2022).
9. Tang-Huau, T.L. *et al.* Human in vivo-generated monocyte-derived dendritic cells and macrophages cross-present antigens through a vacuolar pathway. *Nat Commun* **9**, 2570 (2018).
10. Villar, J. & Segura, E. Decoding the Heterogeneity of Human Dendritic Cell Subsets. *Trends Immunol* **41**, 1062-1071 (2020).
11. Zhang, L. *et al.* Single-Cell Analyses Inform Mechanisms of Myeloid-Targeted Therapies in Colon Cancer. *Cell* **181**, 442-459 e29 (2020).
12. Zhang, F. *et al.* Defining inflammatory cell states in rheumatoid arthritis joint synovial tissues by integrating single-cell transcriptomics and mass cytometry. *Nat Immunol* **20**, 928-942 (2019).
13. Yao, J. *et al.* Genetic landscape and immune mechanism of monocytes associated with the progression of acute-on-chronic liver failure. *Hepatol Int* **17**, 676-688 (2023).
14. Picard, C., Casanova, J.L. & Puel, A. Infectious diseases in patients with IRAK-4, MyD88, NEMO, or IκBα deficiency. *Clin Microbiol Rev* **24**, 490-7 (2011).
15. Conway, D.H., Dara, J., Bagashev, A. & Sullivan, K.E. Myeloid differentiation primary response gene 88 (MyD88) deficiency in a large kindred. *J Allergy Clin Immunol* **126**, 172-5 (2010).
16. Capitani, M. *et al.* Biallelic TLR4 deficiency in humans. *J Allergy Clin Immunol* **151**, 783-790.e5 (2023).
17. Picard, C. *et al.* Clinical features and outcome of patients with IRAK-4 and MyD88 deficiency. *Medicine (Baltimore)* **89**, 403-425 (2010).
18. Picard, C. *et al.* Pyogenic bacterial infections in humans with IRAK-4 deficiency. *Science* **299**, 2076-9 (2003).
19. von Bernuth, H. *et al.* Pyogenic bacterial infections in humans with MyD88 deficiency. *Science* **321**, 691-6 (2008).
20. Cooray, S. *et al.* Neuroinflammation, autoinflammation, splenomegaly and anemia caused by bi-allelic mutations in IRAK4. *Front Immunol* **14**, 1231749 (2023).
21. Hugle, B., Handel, N., Schwarz, K., Borte, M. & Schuster, V. Antinuclear Antibody-Positive Juvenile Idiopathic Arthritis Despite IRAK-4 Deficiency. *J Clin Immunol* **38**, 450-453 (2018).
22. Nishimura, S. *et al.* IRAK4 Deficiency Presenting with Anti-NMDAR Encephalitis and HHV6 Reactivation. *J Clin Immunol* **41**, 125-135 (2021).